# SUSY COLD DARK MATTER DETECTION AT LARGE $\tan\beta$

M. E. GÓMEZ

*Centro de Física das Interacções Fundamentais (CFIF), Departamento de Física, Instituto Superior Técnico, Av. Rovisco Pais, 1049-001 Lisboa, Portugal.*
*E-mail:mgomez@cfif.ist.utl.pt*

J. D. VERGADOS

*Theoretical Physics Division, University of Ioannina,*
*E-mail: vergados@cc.uoi.gr*

We study the direct detection rate for SUSY cold dark m atter (CDM) predicted by the minimal supersymmetric standard model with universal boundary conditions and large values for $tan\beta$. The relic abundance of the lightest supersymmetric particle (LSP), assumed to be approximately a bino, is obtained by including its coannihilations with the next-to-lightest supersymmetric particle (NLSP), which is the lightest s-tau. We find detectable rates in the currently planned experiments for a sector of the parameter space consistent with the cosmological constraint on the LSP relic abundance and the ones imposed by $b \to s\gamma$ and the Higgs searches.

## 1 Introduction

The minimal Supersymmetric extension of the standard model (MSSM) [1] with $R$–parity conservation predicts an stable lightest supersymmetric particle (LSP). Its relic abundance can provide the desirable amount of cold dark matter (CDM) in order to close the Universe [2].

In the present work will concentrate on the more restrictive version of the MSSM, with minimal supergravity (mSUGRA) and gauge unification. We will show how at large values of $\tan\beta$ it is possible to find scenarios such that predicted LSP is detectable in currently planned experiments and its relic abundance falls inside the bounds of cosmological interest.

## 2 The MSSM at large $\tan\beta$ and the $b \to s\gamma$ constraint

Some details on the choice of the MSSM parameter space have already been presented by J.D. Vergados in this conference [6]. Further details are given in Refs. [3,5].

The most two relevant characteristics of the MSSM at large $\tan\beta$ for our study are the relatively low values of the masses of pseudoscalar higgs $m_A$ and the NLSP (the lightest stau in our analysis). The fist is related to the enhancement of the LSP–nucleon scalar cross section at large $\tan\beta$, the second enables coannihilations LSP–NLSP which are required for the prediction of a LSP relic abundance inside the cosmological bounds.

An accurate determination of $m_A$ is crucial for our work. We follow the procedure outlined in ref. [3], which takes into account the full 1–loop potential

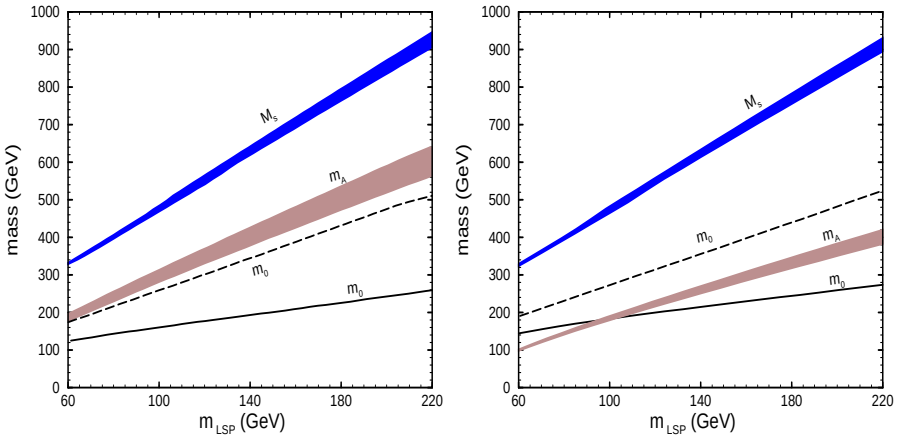


Figure 1. The values of $m_0$, $m_A$ and $M_S$ as functions of $m_{\tilde{\chi}}$ or $m_{\tilde{\chi}}$ for $\tan\beta = 40$ (left) and $\tan\beta = 52$ (right), $\mu > 0$, $A_0 = 0$, the upper boundaries (lower) on the shaded areas and the upper (lower) dashed line corresponds to $m_{\tilde{\tau}_2} = 2 \times m_{\tilde{\chi}}$ ($m_{\tilde{\tau}_2} = m_{\tilde{\chi}}$).

effective potential. Imposing a relation between the LSP and NLSP masses we can find the values of $m_0$ and $M_{1/2}$ corresponding to a certain value of $m_A$. Therefore the GUT values of $M_{1/2}$ and $m_0$ can be traded by the value of $m_A$ and the mass splitting between the LSP and the NLSP $\Delta_{\tilde{\tau}_2} = (m_{\tilde{\tau}_2} - m_{\tilde{\chi}})/m_{\tilde{\chi}}$.

The values of our input parameters in the two scenarios we consider are shown in fig.1. The higher one, $\tan\beta = 52$, corresponds approximately to the unification of the tau and top Yukawa couplings at $M_{GUT}$. The lower value, $tan\beta = 40$, results in a $\sigma^{nucleon}_{scalar}$ smaller by one order of magnitude. $M_S$ is the common SUSY threshold, defined as $M_S = \sqrt{m_{\tilde{t}_1} m_{\tilde{t}_2}}$. The shaded areas correspond to the range of values taken by $m_A$, $M_S$ as $\Delta_{\tilde{\tau}_2}$ ranges from 0 to 1. The area associated with $m_0$ for the same range of $\Delta_{\tilde{\tau}_2}$ is wider as shown by the dashed and solid lines.

The choice $\mu > 0$ leads to a constraint on the parameter space arising from the lower bound on $b \to s\gamma$. As a result the relatively light values for $m_\chi$ and the obtained detection rates are suppressed. Our determination of $BR(b \to s\gamma)$ follows the procedure described in ref. [4]. We complete this analysis by including the appropriate next-to-leading order (NLO) QCD corrections to the SUSY contribution at large values of $\tan\beta$ which recently have become available [7]. The lower limits on $m_\chi$ resulting from this constraint are shown in fig.2.

## 3 LSP relic abundance

Following the considerations of Ref. [3] on the composition of the energy density of the universe in scenarios with vanishing and non vanishing cosmological constant we assume $\Omega_{LSP}h^2$ in the range:

$$0.09 \leq \Omega_{LSP}h^2 \leq 0.22 \tag{1}$$

The composition of the LSP on the model under consideration can be written in the basis of the gauge and Higgs bosons superpartners as:

$$\tilde{\chi} \equiv \tilde{\chi}^0 = C_{11}\tilde{B} + C_{12}\tilde{W} + C_{13}\tilde{H}_1 + C_{14}\tilde{H}_2. \tag{2}$$

In the parameter space we study, $\tilde{\chi}$ is mostly a gaugino with $P = |C_{11}|^2 + |C_{12}|^2 > .95$, with the Bino component being the most dominant one.

The fact that $(\tilde{\chi})$ is mostly a $\tilde{B}$ implies that the main contribution to its annihilation cross section arises from s-fermion (squark, s-lepton) exchange in the t- and u-channel leading to $f\bar{f}$ final states ($f$ is a quark or lepton). If, however, the mass of $\tilde{\chi}$ is close to the one of the NLSP, coannihilations between the two particles must be taken into account [8]. The inclusion these coannihilation effects results in a dramatic reduction of the $(\tilde{\chi})$ relic abundance as the two lightest SUSY particles approach in mass [3,9,10]. We estimate the relic abundance of the LSP $(\tilde{\chi})$, by employing the analysis of Ref.[3] which is appropriate for large $\tan\beta$ and includes coannihilations $\tilde{\chi} - \tilde{\tau}$, suitable for Bino like LSP. To the list of coannihilation channels is given in Table I.

TABLE I. Feynman Diagrams

| Initial State | Final State | Diagrams |
|---|---|---|
| $\tilde{\chi}\tilde{\chi}$ | $\tau\bar{\tau}$ | $t(\tilde{\tau}_{1,2}),\ u(\tilde{\tau}_{1,2})$ |
| | $e\bar{e}$ | $t(\tilde{e}_R),\ u(\tilde{e}_R)$ |
| $\tilde{\chi}\tilde{\tau}_2$ | $\tau h,\ \tau H,\ \tau Z$ | $s(\tau),\ t(\tilde{\tau}_{1,2})$ |
| | $\tau A$ | $s(\tau),\ t(\tilde{\tau}_1)$ |
| | $\tau\gamma$ | $s(\tau),\ t(\tilde{\tau}_2)$ |
| $\tilde{\tau}_2\tilde{\tau}_2$ | $\tau\tau$ | $t(\tilde{\chi}),\ u(\tilde{\chi})$ |
| $\tilde{\tau}_2\tilde{\tau}_2^*$ | $hh,\ hH,\ HH,\ ZZ$ | $s(h),\ s(H),\ t(\tilde{\tau}_{1,2}),\ u(\tilde{\tau}_{1,2}),\ c$ |
| | $AA$ | $s(h),\ s(H),\ t(\tilde{\tau}_1),\ u(\tilde{\tau}_1),\ c$ |
| | $H^+H^-,\ W^+W^-$ | $s(h),\ s(H),\ s(\gamma),\ s(Z),\ c,\ t(\tilde{\nu}_\tau)$ |
| | $\gamma\gamma,\ \gamma Z$ | $t(\tilde{\tau}_2),\ u(\tilde{\tau}_2),\ c$ |
| | $t\bar{t},\ b\bar{b}$ | $s(h),\ s(H),\ s(\gamma),\ s(Z)$ |
| | $\tau\bar{\tau}$ | $s(h),\ s(H),\ s(\gamma),\ s(Z),\ t(\tilde{\chi})$ |
| | $u\bar{u},\ d\bar{d},\ e\bar{e}$ | $s(\gamma),\ s(Z)$ |

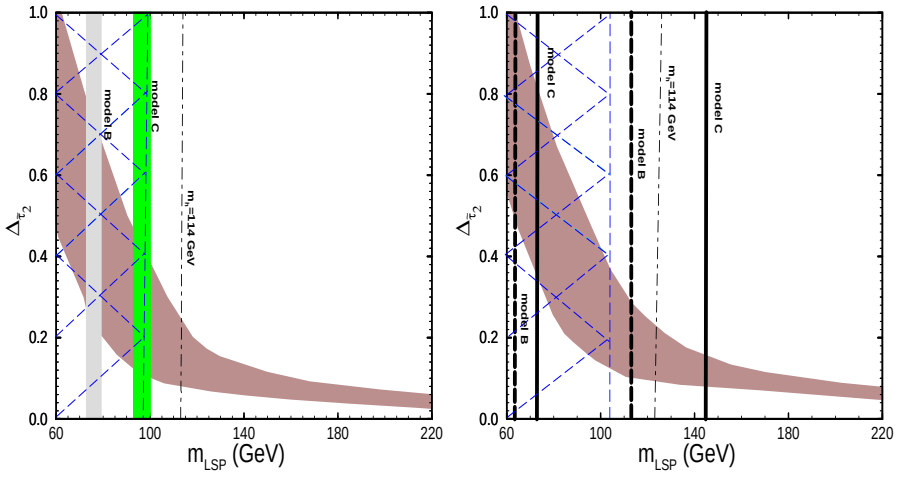


Figure 2. The cosmologically allowed region in the $m_{\tilde{\chi}} - \Delta_{\tilde{\tau}_2}$ plane (shaded area) for $\tan\beta = 40$ (left) and $\tan\beta = 52$ (right). The vertical bands in graph on the left correspond to the bound $\sigma_{scalar}^{(nucleon)} = 4 \cdot 10^{-7} pb$, obtained from figure 2 for both models. The vertical lines on the graph of the right correspond to the bounds $\sigma_{scalar}^{(nucleon)} = 4 \cdot 10^{-7} pb$ (lines towards the right of the graph) and $2 \cdot 10^{-5} pb$ for the models indicated. The marked areas on the left are excluded by $b \to s\gamma$.

We should, at this point, clarify that in the parameter space considered here no resonances in the s–channels were found. In other words the s–channel exchange of A , h, H, Z into $\tilde{\tau}_2\tilde{\tau}_2^*$ never becomes resonant in the parameter space of our analysis. We can see in Fig. 1, however, that a line $mass = 2m_{\tilde{\chi}}$ will be above of the $m_A$ region for the case of $\tan\beta = 52$, while for $\tan\beta = 40$ it will not. However we should emphasize here, that the position the $m_A$ band displayed is Fig.1 respect a line of $mass = 2m_{\tilde{\chi}}$ is very sensitive to small changes in $\tan\beta$ and the values $m_t$,$m_b$ and the GUT values for $A_0$ and $m_0$. Therefore, at the large values of $\tan\beta$ it is possible to find sectors of the space of parameters where $m_A \approx m_{\tilde{\chi}}$, in these cases the the adequate treatment of the Higgs mediated annihilation channels will be determining for an accurate calculation of $\Omega_{LSP}\, h^2$.

The choice of parameter space in the two examples we present is aimed to illustrate the decisive role of $\tan\beta$ in the LSP detection rates as we show in Fig.2. In the two scenarios we choose, annihilation resonant channels are not present and coannihilations are required in order to predict a cosmologically desirable LSP relic abundance.

## 4 LSP–Nucleon Elastic Cross Section

The coherent scattering $\tilde{\chi} + (A, Z) \rightarrow \tilde{\chi} + (A, Z)^*$ can be mediated via s-quarks and neutral Higgs particles (h and H). In our model we find that the Higgs contribution becomes dominant and therefore:

$$\sigma_{scalar}^{nucleon} \propto \left[ f_s^0 - f_s^1 (1 - 2\frac{Z}{A}) \right]^2 , \tag{3}$$

where:

$$f_s^0 = \frac{1}{2}(g_u + g_d) + g_s + g_c + g_b + g_t \tag{4}$$

$$f_s^1 = \frac{1}{2}(g_u - g_d). \tag{5}$$

With:

$$g_{u_i} = [g_h cos\alpha + g_H sin\alpha] \frac{f_{u_i}}{sin\beta}, \quad u_i = u, c, t; \tag{6}$$

$$g_{d_i} = [-g_h sin\alpha + g_H cos\alpha] \frac{f_{d_i}}{sin\beta}, \quad d_i = d, s, b. \tag{7}$$

In the eq, above $\alpha$ is the mixing angle which appear in the diagonalizaton of the $CP$-even Higgs mass matrix, and $g_h,\ g_H$ can be written as:

$$g_h = 4(C_{11}^\star tan\theta_W - C_{11}^\star)(C_{41} \cos\alpha + C_{31} \sin\alpha) \frac{m_N m_W}{m_h^2} \tag{8}$$

$$g_H = 4(C_{11}^\star tan\theta_W - C_{11}^\star)(C_{41} \sin\alpha - C_{31} \cos\alpha) \frac{m_N m_W}{m_H^2}. \tag{9}$$

The last equations gets enhanced as $\tan\beta$ increases, since the electroweak symmetry breaking imposes lower values for the pseudoscalar Higgs mass $m_A$ (see Fig. 1). This implies a lower value for of $m_H$. The changes on $m_h$ are not so important, since its value can only move below an upper bound of about 120-130 GeV . The coefficients $C_{ij}$ depends on the composition of the LSP. For all the values of the $m_{\tilde{\chi}}$, however, reported in the present work the condition $P > .9$ is maintained. It becomes even more stringent, $P > .95$, for $m_{\tilde{\chi}} > 100$ GeV.

The factors $f_{u_i},\ f_{d_i}$ parametrize the quark nucleon matrix element. They depend on the quark model used for the nucleon, we use two different quark models in our calculation denoted as models B and C. Their values along with further details were given in by Vergados [6] and can be found in Ref. [5].

The parameter space leading to predictions of

$$4 \times 10^{-7}\ pb\ \leq \sigma_{scalar}^{nucleon} \leq 2 \times 10^{-5}\ pb \tag{10}$$

is shown in fig.2.

## 5 Conclusions

In summary, we have found that the most popular version of the MSSM with gauge unification and universal boundary conditions at the GUT scale, and a parameter space determined by large values of $\tan\beta$, can accommodate a cosmologically suitable LSP relic abundance and predict detection rates, which can be tested in current or projected experiments.

We should mention that the calculated detection rates can vary by orders of magnitude, depending on the yet unknown LSP mass. Other source of uncertainty comes from estimating the heavy quark contribution in the nucleon cross section. This seems to be under control. We take the difference between the models B and C discussed above as an indication of such uncertainties. They seem to imply uncertainties no more than factors of two.

We believe, therefore, that, concerning the direct LSP detection event rates the main uncertainties come from the fact that the SUSY parameter space is not yet sufficiently constrained. The parameter space may be sharpened by the accelerator experiments, even if the LSP is not found. We should mention here, in particular, the Higgs searches, since, as we have seen, the role of the Higgs particles in direct SUSY dark matter detection is crucial. It is not an exaggeration to say that the underground and accelerator experiments are complementary and should achieve a symbiosis.

This work was supported by the European Union under the contracts RTN No HPRN-CT-2000-00148 and TMR No. ERBFMRX–CT96–0090 and $\Pi ENE\Delta$ 95 of the Greek Secretariat for Research.

## References

1. H.E. Haber and G.L.Kane, Phys. Rep. **117**, 75 (1985).
2. G. Jungman *et al.*,*Phys. Rep.* **267**, 195 (1996).
3. M.E. Gómez, G. Lazarides and C. Pallis, Phys. Rev. D **61** (2000) 123512; M.E. Gómez, hep-ph/0102049.
4. M.E. Gómez, G. Lazarides and C. Pallis, Phys. Lett. **B487** (2000) 313.
5. M. Gómez and J.D. Vergados, hep-ph/00120020.
6. J.D. Vergados and M. Gómez, hep-ph/0105114.
7. C. Degrassi, P. Gambino and G. F. Guidice, JHEP **0012** (2000) 009; M. Carena, D. García, U. Nierste and C. E. Wagner, Phys. Lett. **B499** (2001) 141;
8. K. Griest and D. Seckel, Phys. Rev. **D43** (1991) 3191.
9. M. Drees and M. M. Nojiri, Phys. Rev. **D47** (1993) 376; S. Mizuta and M. Yamaguchi, Phys. Lett. **B298** (1993) 120; P. Gondolo and J. Edsjö, Phys. Rev. **D56** (1997) 1879;
10. J. Ellis, T. Falk and K. A. Olive, Phys. Lett. **B444** (1998) 367; J. Ellis *et al.* Astropart. Phys. **13** (2000) 181 and hep-ph/0102098; R. Arnowitt, B. Dutta and Y. Santoso, hep-ph/0102181.